Computational blood flow simulations and geometric uncertainty quantification in patient-specific aorta-insights

Catarina Reis Fernandes Caseiro Catarino
catarina.catarino@tecnico.ulisboa.pt

Instituto Superior Técnico, Lisboa, Portugal

June 2015

Abstract

The geometric uncertainty of the aortic valve stenosis was quantified in terms of hemodynamic parameters in the thoracic aorta. A 3D patient-specific aorta geometry was used and the valve modelled as an idealized disk at the inlet of the ascending aorta to mimic the calcification of the heart valves. The uncertainty of the random opening radius was characterized by Beta Probability Density Function with a variability of 14% and quantified in the aorta flow development during the cardiac cycle. The stochastic process involved the application of a Non-Intrusive Spectral Projection method which is based on the Polynomial Chaos expansion and uses samples corresponding to 3D time-dependent flow fields obtained from the solution of the unsteady Navier-Stokes equations. The deterministic simulations were validated with reported data of the aorta blood flow. Comparisons have been made between the solutions obtained with Newtonian and non-Newtonian blood viscosity models and the consideration of laminar or turbulent flow. The occurrence of turbulent blood flow was examined for a 3D patient-specific geometry via wall shear stress distribution and turbulent intensity level. The present study revealed that the stenosed valve originates a jet inflow disturbing the flow to a greater degree and generating recirculation regions that reattach further downstream. The stochastic outputs were analysed in terms of hemodynamic parameters with clinical relevance during the cardiac cycle. The radius opening variability led to significant differences at the peak of systole, particularly in the ascending aorta and the brachiocephalic arteries.

Keywords: Blood flow, CFD, Aorta, Patient-specific geometry, Uncertainty quantification, Non-Intrusive Spectral Projection

1. Introduction

Computational Fluid Dynamics (CFD) and Three-Dimensional (3D) imaging techniques have enabled a range of new applications in the study of cardiovascular mechanics in patient-specific models. It gained great importance in the characterization of healthy and pathological situations, design of medical devices, prediction of outcomes from surgeries, diagnosis and treatment planning [1, 2].

The aortic valve stenosis is primarily a disease that affects elderly people and its main cause is the calcification of the heart valves. The majority of the patients presents altered transvalvular pressure gradient, tissue fibrosis, left ventricle hypertrophy and jet formation [3]. Also, clinical findings confirmed the presence of turbulent flow throughout the ascending aorta (AscAo) and brachiocephalic (BC) arteries [4, 5]. Recent studies suggested that the multi disease patterns can lead to an underestimation of the severity of the disease and thus a delayed intervention. Therefore, there are several clinically challenging problems to assess [3]: determine the stage of the aortic valve stenosis; distinguish between moderate and severe stages; estimate a short-term prognosis and study patients with isolated aortic valve stenosis.

Additionally, more powerful computational resources has been providing faster and efficient results which can be obtained in a few hours instead of days to weeks. In the near future, it is believed that medical community will benefit from personalized real time prediction models [6].

However, the confidence of the results is strongly dependent on the level of certainty of the input parameters and it is needed to determine how the input variability may affect the output parameters. Cardiovascular simulations face the problem of uncertainty from several sources including vessel geometry, boundary conditions, material properties and blood viscosity models [7]. The vessel geometry definition depends on the accuracy limit of medical image acquisition, image noise and variations in segmentation methods. Furthermore, the lack of clinical data and *in vivo* experiments influences the

choice of boundary conditions and material properties [7]. Additionally, uncertainty also exists in blood viscosity models. Despite the large number of blood viscosity models, the blood rheology has not yet been fully expressed due to its complexity and dependence on many factors [8].

Several applications of Non-Intrusive Spectral Projection (NISP) technique in cardiovascular system uncertainties have been reported. *Sankaran and Marsden* [7] applied the stochastic collocation method to quantify the effects of geometry and boundary conditions variability on the output parameters using two idealized models (abdominal aortic aneurysm and carotid artery) and a patient-specific geometry from Fontan procedure. It was also pointed out that the choice of the input parameters is crucial to evaluate stochastic space representations of the outputs: the Probability Density Function (PDF) and the Confidence Interval (CI). *Xiu and Sherwin* [9] performed a parametric uncertainty analysis regarding the pulse wave propagation in 37 arteries that represent the largest arteries of the human circulatory system. *Pereira et al.* [8] quantified the uncertainty of random blood viscosity model parameters reporting that the NISP approach is an adequate approach to predict error bar and PDF distribution of different variables in cardiovascular applications.

The present work aims to develop a methodology based on a CFD procedure to accurately simulate blood flow in a 3D patient-specific aorta and to quantify the geometric uncertainty of the radius variability in a case of aortic valve stenosis. The main goal is to contribute to take image-based CFD of cardiovascular flows closer to clinical practice, as it is believed that it can provide additional information of uncertainty quantification which is unavailable in traditional measurement techniques. The computational domain comprises a 3D patient-specific aorta model and a stenosed aortic valve modelled as an idealized perforated disc with a opening radius variability characterized by a Beta PDF distribution. The relative high Reynolds number in the aorta triggers turbulence spots that have been observed during the deceleration phase of the cardiac cycle in the AscAo, see *Fung* [10], especially under pathological conditions such as diseased aortic valves [4, 11]. For these reasons the present calculations have considered turbulent flow together with the Newtonian assumption that is an adequate approach for unsteady flow in a healthy human thoracic aorta.

Next section describes the governing equations and the boundary conditions. After this, validation study is performed to guarantee the results quality. Section 3 deals with the analysis of a patient-specific aorta model obtained from a procedure of medical image segmentation as well as on the comparison between Newtonian and non-Newtonian blood viscosity models and the differences between laminar and turbulent assumptions. This is followed by the geometric uncertainty of the radius variability in a case of aortic valve stenosis, and their quantification in terms of hemodynamic parameters with clinical relevance including the blood flow pressure, velocity and Wall Shear Stress (WSS) fields in the aorta. The paper ends with the summary conclusions.

2. Numerical Model

The unsteady Navier-Stokes equations described the blood flow behaviour under the continuum assumption. For the turbulent assumption, the K-Omega Shear Stress Transport (SST) turbulence model was used. The CFD simulations were performed in STAR-CCM+® during 2 cardiac cycles discretized by 100 time-steps per cardiac cycle. Second order spatial discretization schemes and implicit second order for time-stepping were used.

2.1. Boundary conditions

Blood flow was assumed to be a Newtonian or a non-Newtonian fluid and incompressible with density $\rho = 1060$ kg/m^3. In the Newtonian case, blood dynamic viscosity $\mu = 0.0035$ Pa $\cdot$ s is independent of the shear rate. For the non-Newtonian approach, the Carreau model was used with parameters $\mu_0 = 0.0456$ Pa $\cdot$ s, $\mu_\infty = 0.0032$ Pa $\cdot$ s, $\lambda = 10.03$ s and $n = 0.344$ being its apparent viscosity decreasing as shear rate increases, see *Gambaruto et al.* [12]. In the present study, two different physiological states from experimental data [13] were considered: rest and exercise conditions. To simulate a realistic cardiac cycle, a time-dependent mass flow rate was applied at the AscAo inlet. In rest conditions, the mean cardiac output was 3.7 L/min with a heart rate of 47 beats per minute (bpm) and a period of 1.27 s. In exercise conditions, the mean cardiac output was 13.5 L/min with a heart rate of 141 bpm and a period of 0.43 s. Outflow waveforms were imposed at the BC, left common carotid (LCC), left subclavian (LSA) and descending aorta (DescAo) arteries according to specified fractions of the inflow which are represented in Table 1. The vessel wall was assumed to be rigid with the no-slip condition.

Table 1: Total percentage of flow through the various branches under rest and exercise conditions

	AscAo	BC	LCC	LSA	DescAo
Rest	100%	17%	8%	10%	65%
Exercise	100%	25%	5%	11%	59%

2.2. Validation

For validation purposes, a test case was taken from *Cito et al.* [13] in which a patient-specific aortic coarctation model was studied under rest and exercise physiological conditions in order to predict the blood pressure gradient across the coarctation. Three different volumetric meshes were constructed with tetrahedral or polyhedral elements: 280k cells with 5 prismatic layers, 515k cells with 3 prismatic layers and 1.3M cells with 5 prismatic layers. Local refinements were performed in the outlets as well as an extrusion mesh with appropriate stretching values. The blood flow was modelled as being incompressible with $\rho = 1000$ kg/m^3, laminar and Newtonian with $\mu = 0.004$ Pa $\cdot$ s. Boundary conditions at inlet and outlets were the ones described before in Section 2.1. Results were analysed at the four main phases of the cardiac cycle: acceleration $t1$, peak of systole $t2$, deceleration $t3$ and diastole $t4$ as shown in Figure 1.

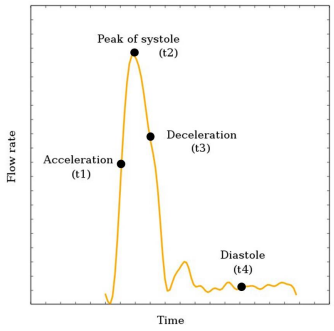

Figure 1: Four main phases of the cardiac cycle

The pressure gradient results in Figure 2 show that a polyhedral mesh is a better alternative over the tetrahedral mesh represented with a red dotted line in rest conditions. In addiction, a mesh of 1.3 million elements and 5 prismatic layers is the one that best fits the values of *Cito et al.* in rest and exercise conditions. After this analysis, all the validation simulations were performed using this mesh. Analysing Figures 2 and 3 for rest and exercise physiological conditions respectively, the pressure gradient starts rising steadily and reach a peak representing the systolic peak. Then, decline and reach the bottom of the graphic corresponding to the transition from deceleration phase to diastole. In the diastole, the pressure gradient fluctuates slightly around zero. The greater difference between rest and exercise conditions is the peak of pressure gradient which is 30 mmHg and 200 mmHg, respectively.

Figure 4 allows a visual comparison of the WSS distribution in rest and exercise conditions during the cardiac cycle. In both cases, the WSS has an evolution in agreement with the imposed inlet flow

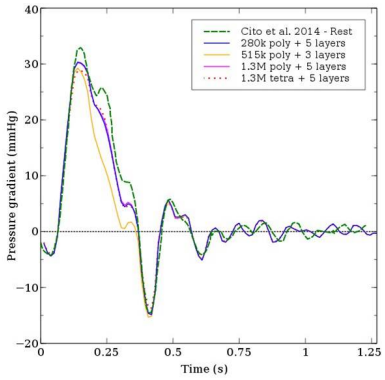

Figure 2: Pressure gradient under rest conditions compared to *Cito et al. 2014*

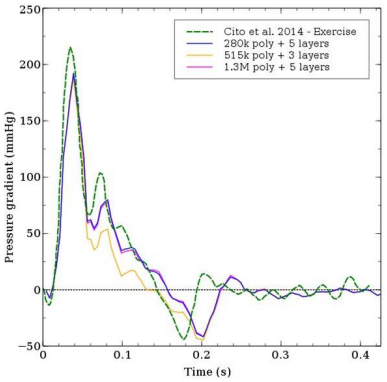

Figure 3: Pressure gradient under exercise conditions compared to *Cito et al. 2014*

rate and the coarctation act like a stenosis inducing a region of very high WSS at $t2$ and $t3$ [5]. Besides this zone, the areas with highest WSS are located in the three upper branches specially in LCC outlet that is the one with the smallest area. Moreover, the WSS is also high on the outer wall of the aortic arch and in AscAo inlet where the flow rate. The areas with the lowest WSS are the entrance of the three upper branches highlighted with a black circle and the inner wall of DescAo. Along the DescAo, the WSS distribution has a complex pattern for both cases. As expected, the WSS is lower in rest conditions when compared with exercise state. The results are according to physiological patterns in the presence of aortic coarctation [14]. Therefore, the model can be said to be validated for the purpose of the present work.

3. Medical Image Segmentation

A patient-specific aorta geometry was created from medical imaging data provided by Faculdade de Medicina - Universidade de Lisboa (*A. G. Almeida, personal communication, 2014*). The medical imaging data set was obtained from a Computerized Tomography Angiography (CTA) using

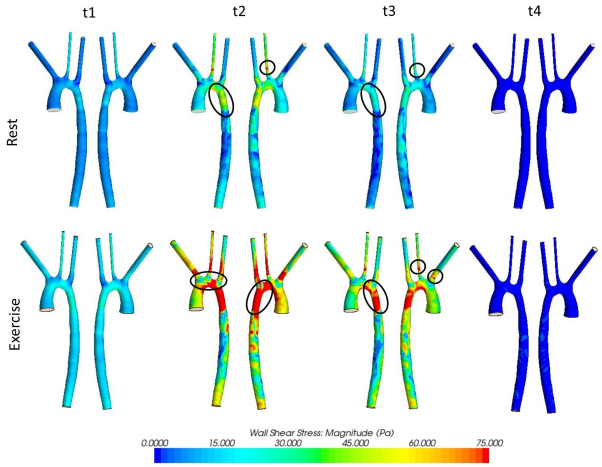

Figure 4: WSS distribution during the cardiac cycle for rest and exercise conditions

a Philips scanner in helix modality with non-ionic contrast injection. The DICOM files were composed by 710 slices from neck to foot with voxel size $0.59 \times 0.59 \times 1$ mm^3, 2 mm slice thickness and 1 mm spacing. Although the *ITK-SNAP* software was chosen for the medical image segmentation, it involved several other steps of surface repair and smoothing. According to *Yushkevich et al.* [15], *ITK-SNAP* tool demonstrates a significant efficiency and excellent reliability segmentation with the capacity of segment structures directly into 3D geometries. In a first stage, the DICOM image sequence was imported into *ImageJ* and the images were cropped to only select the region of interest by removing noise and undesired features. In *ITK-SNAP*, the segmentation task starts with image contrast adjustment and then contour expansion is performed during several iterations under the influence of evolution parameters. In *MeshLab*, surface mesh repairing and a Taubin smooth were applied to construct an acceptable realistic geometry. The 3D model obtained is the aorta artery with the inlet AscAo and the four main outlets: DescAo, BC, LCC and LSA arteries as shown in Figure 5. It has a characteristic volume of 1.67×10^{-4} m^3 and defines the computational domain. The aortic valve stenosis was modelled by creating an idealized disk with a hole at center of the AscAo and it became the new AscAo inlet (see Figure 6). One major aspect is that an on/off modality was chosen to model the aortic valve opening and closure. Particularly, the valve was opened for 0.6 s and closed during 0.67 s associated with the diastolic time.

A volumetric mesh with 1.3 million polyhedral elements with 5 prismatic layers was constructed. Local refinements were performed in the outlets as well as an extrusion mesh with appropriate stretching values.

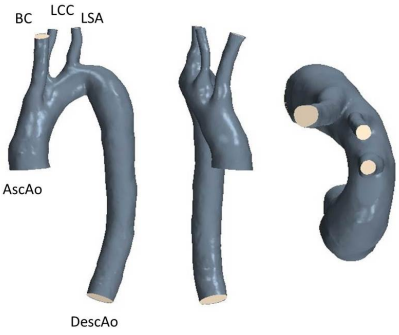

Figure 5: 3D model of aorta in coronal (left), sagittal (center) and axial (right) views

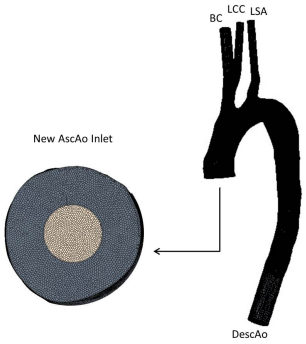

Figure 6: Representation of the 3D volumetric mesh highlighting the new AscAo inlet

4. Deterministic Flow Results

The 3D patient-specific aorta blood flow was analysed in rest and exercise conditions assuming Newtonian and non-Newtonian blood viscosity models (see Section 2.1). Figure 7 shows that the largest differences of WSS magnitude in rest conditions between Newtonian and non-Newtonian models result from local effects mainly in the outer wall of the DescAo outlet and it does not affect the inlet and upper branches. Probably, associated with regions of low strain rate, low velocity and low WSS. During acceleration $t1$ and peak of systole $t2$, differences can achieve 10% whereas in deceleration $t3$, 25% of difference can be obtained and it is the most affected cardiac phase. It is concluded that a non-Newtonian blood viscosity model is not of great significance for the purpose of this study. Hence, the Newtonian blood viscosity model appears to be a reasonable approximation for analysing blood flow in large arteries with time-dependent boundary conditions. This is coherent with the results reported by [16].

An idealized pathological situation was investigated, more precisely a moderate and a severe case

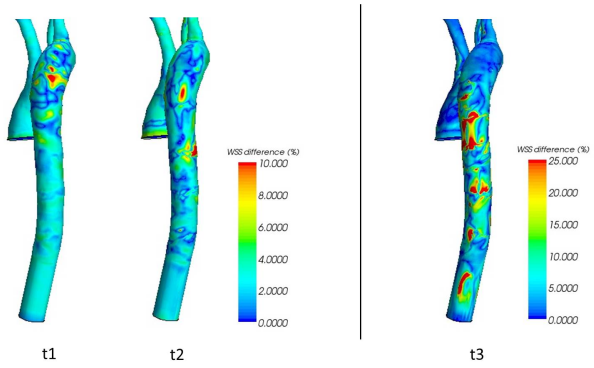

Figure 7: Absolute difference of WSS magnitude between Newtonian and Non-Newtonian blood models

of aortic valve stenosis highlighting the differences between laminar and turbulent assumptions. Figure 8 shows the differences between laminar and turbulent assumptions. For the same flow rate, the turbulent flow originates more frictional losses causing higher WSS, four times higher than in the laminar regime, focused in the AscAo artery. The results obtained demonstrate that turbulent effects are extremely important and should be taken into account in the study of aortic valve stenosis.

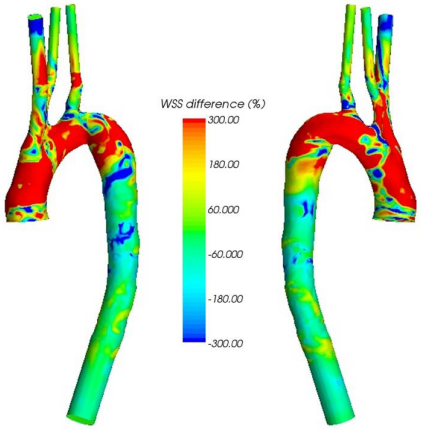

Figure 8: Absolute difference of WSS magnitude between laminar and turbulent conditions in the deceleration phase $t3$

Furthermore, it is verified that the deceleration $t3$ is the part of the cardiac cycle more susceptible to the development of turbulence. In 1997, *Fung* [10] pointed out that turbulence is mainly observed during the deceleration phase of the cardiac cycle when there are more instabilities due to the effect of an adverse gradient. Figure 9 shows the turbulent intensity along the 3D aorta model for this time period for a moderate case of aortic valve stenosis. The turbulent perturbations are dominant in the AscAo, particularly in cut-plane D after the jet with an intensity of 50%. It propagates through the aortic arch and then relaminarization occurs downstream in cut-plane G.

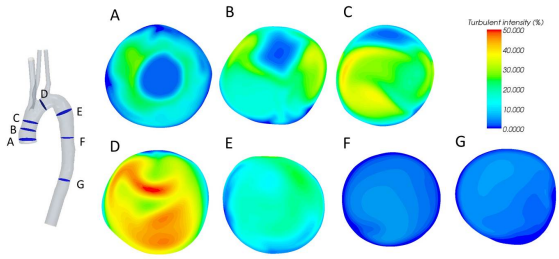

Figure 9: Turbulent intensity on selected cut-planes (A,B,C,D,E,F,G) in the deceleration phase $t3$ for a moderate case

5. Stochastic Process

5.1. Methods

The goal of the uncertainty quantification analysis is to evaluate the effects of the orifice radius variability of an idealized moderate aortic valve stenosis on output parameters, namely pressure, velocity and WSS during the cardiac cycle. Thus, the radius of the aortic valve orifice was taken as the random variable ξ with a semi-circular Beta PDF distribution, with a mean value of 0.6675 cm, standard deviation of 0.02375 cm and $\alpha = \beta = 3/2$. It corresponds to a variability of 14% in the opening radius at the AscAo inlet. Moreover, the ensemble average orifice opening radius of 0.6675 cm corresponds to an area blockage of 77% which is a moderate obstruction. The 3D patient-specific geometry with the new AscAo inlet was constructed to mimic the calcification of heart valves (see Figure 6). Blood flow was assumed to be Newtonian with a turbulent assumption in rest conditions (see Section 2.1).

Deterministic simulations were performed for 3, 5, 7 and 9 quadrature points which are specific points resulting from the characteristic random variable distribution. Each simulation involved a process of changing the inlet of the aortic geometry according to the desired radius. Since it involved a new geometry, the (x,y,z) coordinates of the points in the mesh of the 3D patient-specific model changed slightly. In an attempt to guarantee the maximum accuracy possible, the results of the simulations were interpolated into a common and more refined mesh with 1.8 million elements. The time-dependent pressures at the inlet and at the four outlets were extracted as well as the pressure, the velocity and the WSS fields over the 3D model. The outputs of the deterministic simulations were analysed at four time periods of the cardiac cycle (see Figure 1). After the post processing, the stochastic outputs were quantified using the already mentioned stochastic space representations.

A convergence analysis was performed to assess

the stochastic results dependence on the polynomial degree and on the number of deterministic samples. The PDFs of the time-dependent pressures at the selected five locations at four time periods of the cycle were post-processed and analysed in detail for all deterministic points and all degrees. The stochastic solution variable was characterized by a PDF which describes the likelihood of a random variable to assume a given value and the integral over its entire area is always equal to one. Moreover, the Kullback−Leibler divergence D_{KL}, which is a measure of the difference between two probability distributions, was also calculated to find the best approximation to the output results [17].

5.2. Results

Figure 10 is an example of the convergence study with the PDF of the pressure at the AscAo inlet at time instance $t3$. Considering the 9 points, it is observed that PDFs obtained with a 6^{th} order polynomial and a 7^{th} order polynomial are virtually identical. Table 2 shows the Kullback−Leibler divergence results where the 6^{th} order polynomial with 9 points is compared with the other polynomial degrees. It is verified that the $D_{KL}(P, Q7)$ is one order of magnitude lower that the remaining results.

From the obtained PDFs and the Kullback−Leibler divergence criterion, it is concluded that a 6^{th} polynomial degree obtained with 9 quadrature points is enough to accurately describe the output variables.

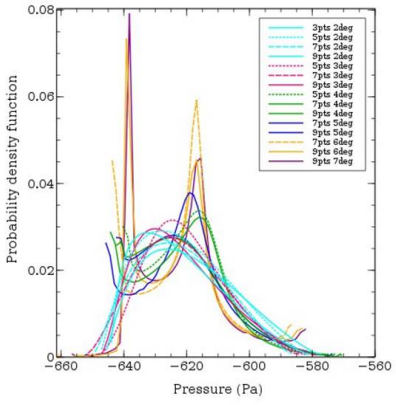

Figure 10: PDF of the pressure at the AscAo inlet at time period $t3$

The pressure error bars for a 95% CI were analysed at AscAo inlet as well as at BC, LCC, LSA and DescAo outlets. The results show that the aortic valve radius variation has a dominant effect on pressure between the peak of systole $t2$ and the deceleration phase $t3$ where the error bar is larger in most cases.

Table 2: Kullback−Leibler divergence considering the 9 points and P as the PDF obtained with a 6^{th} order polynomial and Q2, Q3, Q4, Q5 and Q7 as the 2^{nd}, 3^{rd}, 4^{th}, 5^{th} and 7^{th} polynomial degrees, respectively.

	(P,Q2)	(P,Q3)	(P,Q4)	(P,Q5)	(P,Q7)
D_{KL}	0.2483	0.2742	0.2314	0.2358	0.0322

However, the variability in the acceleration phase $t1$ and in the diastole $t4$ is insignificant and it is verified that the range of PDF of pressure is approximately 0.7% at these time periods. Figure 11 shows the stochastic results of the mean pressure with the error bar for a 95% CI at BC outlet. The pressure at the BC outlet is the most affected by the uncertainty with a maximum variability of about 55% which corresponds to a difference of 3 mmHg in the range [4 mmHg,−7.5 mmHg].

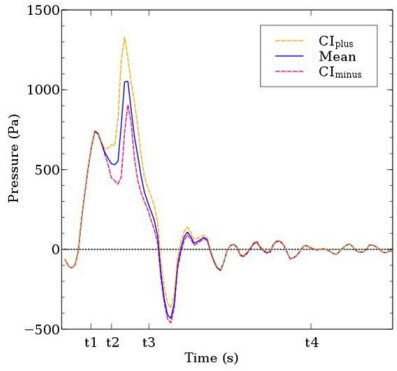

Figure 11: Error bar for a 95% CI at the BC outlet

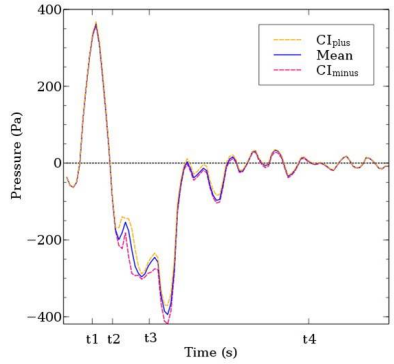

Figure 12: Error bar for a 95% CI at the LSA outlet

On the other hand, the pressures at the AscAo inlet, at the LCC and at the LSA (see Figure 12) are

less influenced with around 25% of maximum variation. Also, it is verified that the error bar is negligible for a 95% CI so the pressure at the DescAo outlet has no influence on the propagation of the radius variability. Figure 13 shows local PDFs of the pressure at the BC artery at time instants $t2$ and $t3$.

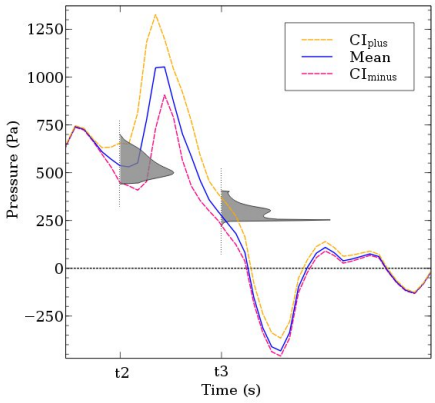

Figure 13: Error bar for a 95% CI at BC outlet with local PDFs at $t2$ and $t3$

Figure 23 shows that in the acceleration phase $t1$ the pressure increases steadily up to 1500 Pa in the AscAo. At the peak of systole $t2$ a region of very high pressure remains on the BC outlet and on the mid-ascending aorta due to the jet effect. In the deceleration period $t3$, the descending aorta presents positive values while the ascending aorta has negative pressure inducing an adverse pressure gradient. For the sake of clearing, the pressure was set to vary around a reference value of 100 mmHg=13300 Pa localized in the DescAo outlet.

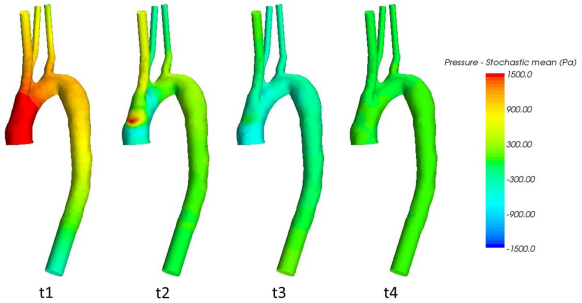

Figure 14: Stochastic mean of the pressure field

Comparing Figures 15 and 16, it is observed that the pressure is highly affected by the radius uncertainty during the peak of systole $t2$. The CV is very high at diastole $t4$ because its mean value is almost zero. Therefore, at the peak of systole $t2$, pressure dispersion occurs mainly in the AscAo and BC arteries reaching CVs from 40% to 100%. During deceleration $t3$, CV can also achieve 100% but focused on a region of the AscAo and in the end of BC artery.

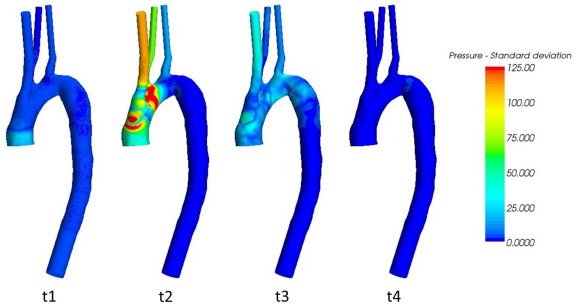

Figure 15: Standard deviation of the pressure field

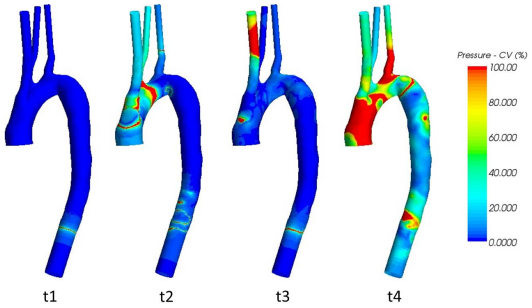

Figure 16: Coefficient of variation of the pressure field

In Figure 17, the jet evolution during three time instances of the cardiac cycle is observed. More precisely, the jet starts emerging at $t1$, the maximum velocity intensity of more than 1.75 m/s is achieved during the peak of systole $t2$ and then decreases slowly until the diastole $t3$. Additionally, the jet of fluid impinges in the outer wall of the AscAo causing flow recirculation in the inner curvature that is evident in $t2$ and $t3$.

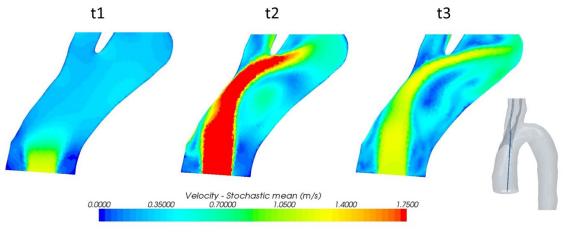

Figure 17: Stochastic mean of the velocity field on a specific cut-plane of the AscAo

Figure 18 shows the development of the jet on three selected cut-planes (A,B,C) along the AscAo where it is clear that the jet really impinges on the wall and hence originates the formation of two vortex rings at A and B during $t2$. After this, the

jet intensity decreases at time $t3$. The vortex rings instability is an indication of the transition to turbulent regime [18]. The values of the CV show a dispersion relative to the mean of about 50% localized in the recirculation region and at the entrance of BC during $t2$ and $t3$ (see Figure 19).

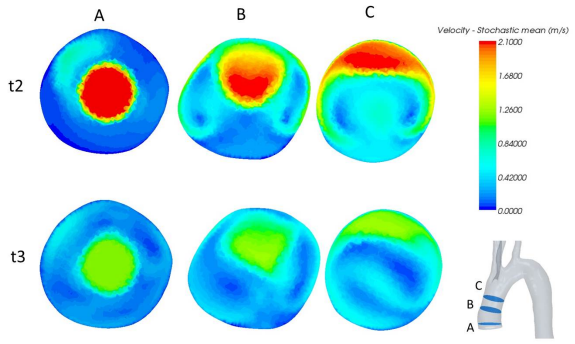

Figure 18: Stochastic mean of the velocity field on three selected cut-planes (A,B,C) along the AscAo

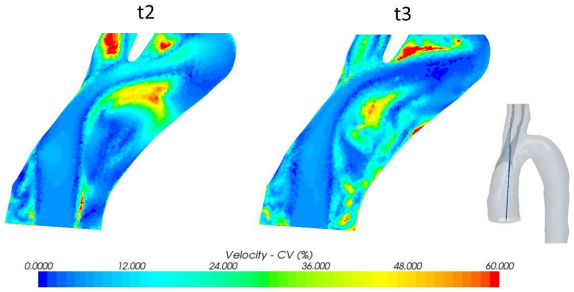

Figure 19: Coefficient of variation of velocity field

Taking a look at Figure 20, it can be seen that the maximum WSS occurs at the peak of systole $t2$ in the mid-ascending aorta as a consequence of the jet effect on the wall. Figure 21 shows large standard deviation values at the AscAo and around the aortic arch during $t2$ and $t3$ due to the same reason.

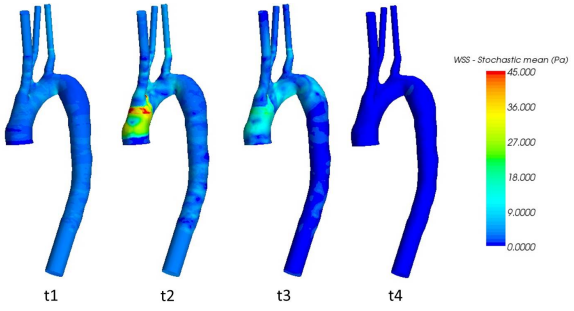

Figure 20: Stochastic mean of WSS field

In Figure 22, the CV of WSS field appears to evolute progressively from the AscAo to aortic arch

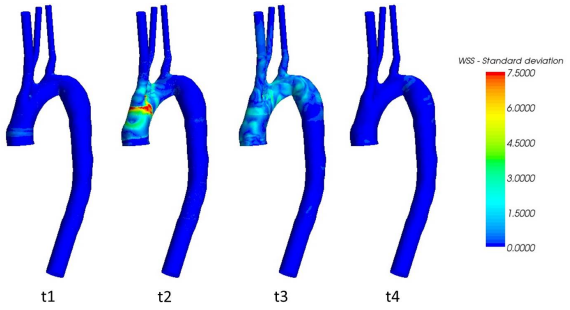

Figure 21: Standard deviation of WSS field

and then to DescAo. Thus, one can say that the radius variability propagates during the cardiac cycle. Once again, the very high values during diastole $t4$ can not be interpreted because its mean value is almost zero. However, at $t2$ and $t3$, CV varies between 40% and 60% which are really relevant results to the medical community.

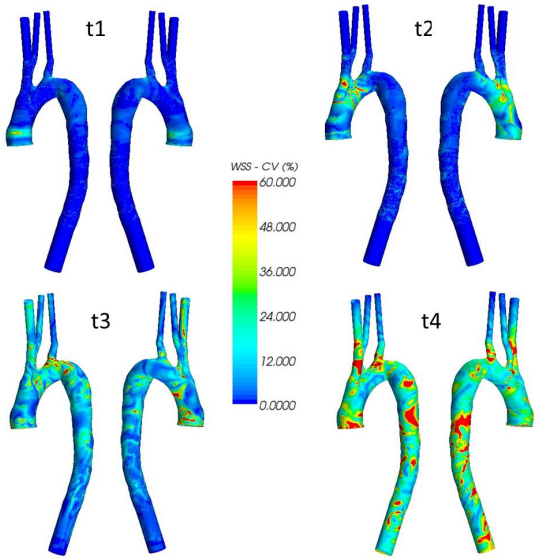

Figure 22: Coefficient of variation of the WSS field

The random opening influences mostly the AscAo and the BC arteries at the peak of systole $t2$. Pressure, velocity and WSS fields show a typical dispersion relative to the mean of about 50%. In general, the radius variability led to significant differences in several hemodynamic parameters with clinical relevance mainly due to the inlet jet flow that induces highly localized pressure and WSS causing a recirculation bubble and vortex rings.

6. Conclusions

In this work, it was developed a methodology based on a CFD procedure to accurately simulate blood flow in a 3D patient-specific aorta and to

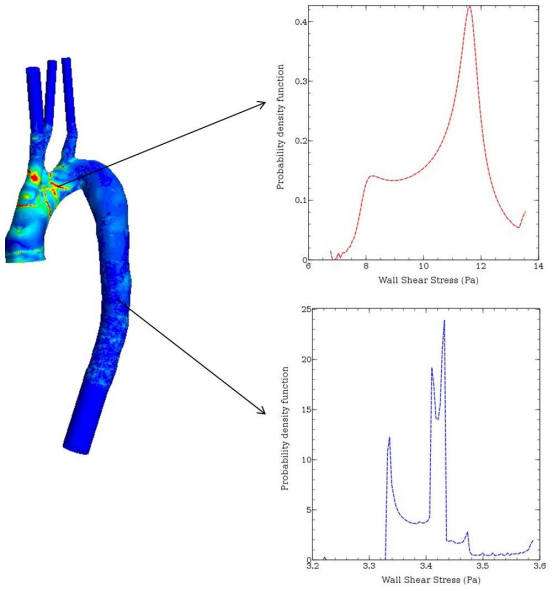

Figure 23: PDFs of WSS field at two distinct points at the peak of systole $t2$

quantify the geometric uncertainty of the opening radius in a case of moderate aortic valve stenosis. The blood flow was described by the 3D unsteady Navier-Stokes equations using the commercial software STAR-CCM+®.

A medical image segmentation procedure was established and correctly performed to obtain the 3D patient-specific aorta geometry that defined the computational domain. The patient-specific aortic blood flow was obtained considering Newtonian and non-Newtonian blood viscosity models. The pressure drop between the AscAo inlet and the DescAo outlet was virtually the same denoting small differences due to high strain rate in large arteries. In regions of low strain rate there were local differences of WSS. Thus, Newtonian blood viscosity model appeared to be a reasonable approximation for analysing blood flow in the aorta with time-dependent boundary conditions.

The aortic valve stenosis, modelled by an idealized disk, created a jet flow surrounded by a complex recirculating flow in the AscAo inlet. The jet impinged on the vessel wall and originated highly localized pressure and WSS. The patient-specific aortic blood flow was calculated considering laminar and turbulent flow. The results demonstrated turbulent effects particularly in the deceleration period $t3$ of the cardiac cycle where turbulent intensity reached 50% in regions surrounding the jet.

The geometric uncertainty of the radius variability of in a case of aortic valve stenosis was quantified using a stochastic process that involved the application of the NISP approach based on the PC expansion. The radius of the disk was taken as the random variable with a characteristic semi-circular Beta PDF. A convergence study was performed and it was concluded that a 6^{th} polynomial degree obtained with 9 quadrature points was enough to accurately describe the output variables.

In general, the pressure error bars for a 95% CI displayed its maximum at the BC outlet at $t2$ achieving a variation of 55% from the mean pressure which corresponded to a difference of 3 mmHg in the range $[4, -7.5]$ mmHg. The pressure and velocity PDFs obtained at different locations and different time instants of the cardiac cycle showed the highest variability at the peak of systole $t2$, particularly in the AscAo and the BC arteries. Typical CV values of 50% were found in these regions denoting that the radius variability led to significant differences in several hemodynamic parameters with clinical relevance. Furthermore, the CV of the WSS field appeared to propagate through the cardiac cycle varying between 40% to 60%.

The geometric uncertainty is characterized by 14% of the disk orifice variability at the AscAo inlet. The ensemble average orifice opening radius of 0.6675 cm corresponds to an area blockage of 77% which corresponds to a moderate obstruction. The present analysis for a more severe case will give rise to larger error bars and variabilities.

Acknowledgements

The author would like to thank Prof. Fausto Pinto and Prof. Ana Almeida (Faculdade de Medicina - Universidade de Lisboa) for providing the medical image data used in this study as well as Prof. Renato Jorge and Prof. Marco Parente (Faculdade de Engenharia - Universidade do Porto) for introducing medical segmentation practices during 3 days in Porto.

References

[1] Charles A Taylor and CA Figueroa. Patient-specific modeling of cardiovascular mechanics. *Annual Review of Biomedical Engineering*, 11:109–134, 2009.

[2] Charles A Taylor and JD Humphrey. Open problems in computational vascular biomechanics: hemodynamics and arterial wall mechanics. *Computer Methods in Applied Mechanics and Engineering*, 198(45):3514–3523, 2009.

[3] Sebastian Herrmann, Stefan Störk, Markus Niemann, Volkmar Lange, Jörg M Strotmann, Stefan Frantz, Meinrad Beer, Stefan Gattenlöhner, Wolfram Voelker, Georg Ertl, et al. Low-gradient aortic valve stenosis: myocardial fibrosis and its influence on function and outcome. *Journal of the American College of Cardiology*, 58(4):402–412, 2011.

[4] Paul D Stein and Hani N Sabbah. Turbulent blood flow in the ascending aorta of humans with normal and diseased aortic valves. *Circulation Research*, 39(1):58–65, 1976.

[5] FPP Tan, A Borghi, RH Mohiaddin, NB Wood, S Thom, and XY Xu. Analysis of flow patterns in a patient-specific thoracic aortic aneurysm model. *Computers & Structures*, 87(11):680–690, 2009.

[6] Bin He, Richard Baird, Robert Butera, Aniruddha Datta, Steven George, Bruce Hecht, Alfred Hero, Gianluca Lazzi, Raphael C Lee, Jie Liang, et al. Grand challenges in interfacing engineering with life sciences and medicine. *Biomedical Engineering, IEEE Transactions on*, 60(3):589–598, 2013.

[7] Sethuraman Sankaran and Alison L Marsden. A stochastic collocation method for uncertainty quantification and propagation in cardiovascular simulations. *Journal of Biomechanical Engineering*, 133(3):031001, 2011.

[8] JMC Pereira, JP Serra e Moura, AR Ervilha, and JCF Pereira. On the uncertainty quantification of blood flow viscosity models. *Chemical Engineering Science*, 101:253–265, 2013.

[9] Dongbin Xiu and Spencer J Sherwin. Parametric uncertainty analysis of pulse wave propagation in a model of a human arterial network. *Journal of Computational Physics*, 226(2):1385–1407, 2007.

[10] Yuan Cheng Fung. *Biomechanics: circulation*. Springer Science & Business Media, 1997.

[11] Davide Ambrosi, Alfio Quarteroni, and Gianluigi Rozza. *Modeling of physiological flows*, volume 5. Springer Science & Business Media, 2012.

[12] Alberto M Gambaruto, João Janela, Alexandra Moura, and Adélia Sequeira. Sensitivity of hemodynamics in a patient specific cerebral aneurysm to vascular geometry and blood rheology. *Mathematical Biosciences and Engineering: MBE*, 8(2):409–423, 2011.

[13] Salvatore Cito, Jordi Pallarés, and Anton Vernet. Sensitivity analysis of the boundary conditions in simulations of the flow in an aortic coarctation under rest and stress conditions. In *Statistical Atlases and Computational Models of the Heart. Imaging and Modelling Challenges*, pages 74–82. Springer, 2014.

[14] John F Ladisa, C Alberto Figueroa, Irene E Vignon-Clementel, Hyun Jin Kim, Nan Xiao, Laura M Ellwein, Frandics P Chan, Jeffrey A Feinstein, and Charles A Taylor. Computational simulations for aortic coarctation: representative results from a sampling of patients. *Journal of Biomechanical Engineering*, 133(9):091008, 2011.

[15] Paul A Yushkevich, Joseph Piven, Heather Cody, Sean Ho, James C Gee, and Guido Gerig. User-guided level set segmentation of anatomical structures with ITK-SNAP. In *Insight Journal, Special Issue on ISC/NA-MIC/MICCAI Workshop on Open-Source Software*, 2005.

[16] AD Caballero and S Laín. Numerical simulation of non-Newtonian blood flow dynamics in human thoracic aorta. *Computer Methods in Biomechanics and Biomedical Engineering*, 18(11):1200–1216, 2015.

[17] John R Hershey and Peder A Olsen. Approximating the Kullback-Leibler divergence between Gaussian mixture models. In *Acoustics, Speech and Signal Processing, 2007. ICASSP 2007. IEEE International Conference on*, volume 4, pages IV–317. IEEE, 2007.

[18] SJ Sherwin and Hugh M Blackburn. Three-dimensional instabilities and transition of steady and pulsatile axisymmetric stenotic flows. *Journal of Fluid Mechanics*, 533:297–327, 2005.